Molecular Biology of the Cell
Vol. 18, 4013–4023, October 2007

Expansion of Chromosome Territories with Chromatin Decompaction in BAF53-depleted Interphase Cells[D]

Kiwon Lee,* Mi Jin Kang,* Su Jin Kwon,* Yunhee Kim Kwon,† Ki Woo Kim,‡ Jae-Hwan Lim,§ and Hyockman Kwon*

*Department of Bioscience and Biotechnology, Hankuk University of Foreign Studies, Yongin 449-791, Korea; †Department of Biology, Kyunghee University, Seoul 130-701, Korea; ‡National Instrumentation Center for Environmental Management, Seoul National University, Seoul 151-921, Korea; and §Department of Biology, Andong National University, Andong 760-749, Korea

Submitted May 11, 2007; Revised July 10, 2007; Accepted July 13, 2007
Monitoring Editor: Wendy Bickmore

Chromosomes are compartmentalized into discrete chromosome territories during interphase in mammalian cells. A chromosome territory is generated by the tendency of chromatin to occupy the smallest shell volume, which is determined by the polymeric properties and interactions of the internal meshwork of the chromatin fiber. Here, we show that BAF53 knockdown by small interfering RNA interference led to the expansion of chromosome territories. This was accompanied by a reduction in chromatin compaction, an increase in the micrococcal nuclease sensitivity of the chromatin, and an alteration in H3-K9 and H3-K79 dimethylation. Interestingly, the BAF53 knockdown cells suffer a cell cycle defect. Despite the significant irregularity and decompaction of the polynucleosomes isolated from the BAF53 knockdown cells, the chromatin loading of H1 and core histones remained unaltered, as did the nucleosome spacing. The histone hyperacetylation and down-regulation of BRG-1, mBrm, and Tip49, the catalytic components of the SWI/SNF complex and the TIP60 complex, respectively, did not expand chromosome territories. These results indicate that BAF53 contributes to the polymeric properties and/or the internal meshwork interactions of the chromatin fiber probably via a novel mechanism.

INTRODUCTION

Chromosomes in interphase cells are confined to mutually exclusive chromosome territories (CTs) located in the nucleus (Schardin *et al.*, 1985). A chromosome can be thought of as a long polymer chain with a tendency to occupy a particular envelope volume, which is defined as the volume of the shell containing all of the chromatin (Kleckner *et al.*, 2004). This suggests that the CT is a cytological manifestation of this envelope. Two parameters may be used to determine the envelope volume of a chromosome. First, the polymeric properties of a chromatin fiber, such as its stiffness and contour length, could be used to determine the envelope volume. A long polymer chain occupies a greater volume when it becomes stiffer and/or extended. Thus, histone modification, differential association of nonhistone architectural components, or histone elimination may lead to alterations of the envelope volume. The interactions of the internal meshwork constitute another parameter that limits the envelope volume of a polymer. In chromatin, interactions between adjacent chromatin fibers and/or the anchoring of the chromatin fiber into a protein-rich scaffold provide an internal meshwork whose interactions constrain the expansion of the chromatin.

In particular, these interactions of the internal meshwork play a key role in determining the higher-order organization of chromatin within the subdomain. The architecture of the CT has been described as a meshwork of compact chromosomal subdomains that are channeled by an intersubdomain space (Cremer and Cremer, 2001). Chromosomal subdomains have been visualized as interconnected, bead-like structures with diameters ranging from 100 to 450 nm (Belmont and Bruce, 1994). The multiloop subcompartment model and the chromonema model have been proposed as possible models for the structure of the chromosomal subdomain. The multiloop subcompartment model proposes a ~1-Mb chromatin domain built up like a rosette with a proteineous backbone structure at the center that holds a series of chromatin-loop domains of ~100 kb (Munkel *et al.*, 1999). On the other hand, the chromonema model suggests that the chromatin constructs a series of progressive folds via intrafiber interactions in order to generate a series of thicker fibers: 30 nm, 60–80 nm, and 100–130 nm in thickness (Belmont and Bruce, 1994). However, the higher-order organization of chromatin within the subdomain has not yet been fully resolved, in part due to the lack of knowledge regarding the interactions of the internal meshwork.

BAF53 is an actin-related protein (Arp) found in many mammalian chromatin-modifying complexes. The SWI/SNF complex is one such complex that alters the spatial organization of nucleosomes in an ATP-dependent manner (Kwon *et al.*, 1994; Zhao *et al.*, 1998). The TIP60 complex is a chromatin-modifying complex that exhibits histone acetyl transferase (HAT) activity (Ikura *et al.*, 2000). Nucleosome remodeling or histone acetylation alone, followed by the

This article was published online ahead of print in *MBC in Press* (http://www.molbiolcell.org/cgi/doi/10.1091/mbc.E07–05–0437) on July 25, 2007.

[D] The online version of this article contains supplemental material at *MBC Online* (http://www.molbiolcell.org).

Address correspondence to: Hyockman Kwon (hmkwon@hufs.ac.kr).

Abbreviations used: CT, chromosome territory; HAT, histone acetyl transferase; FISH, Fluorescence in situ hybridization; MNase, micrococcal nuclease; FACS, fluorescence-activated cell sorting.

subsequent recruitment of other HATs, histone methyltransferases, or nonhistone architectural components, could alter the polymeric properties of the chromatin fiber. Intriguingly, all chromatin-modifying complexes with BAF53 contain stoichiometric amounts of β-actin, which raises the possibility that they form a heterodimer that acts as a nucleation center for the oligomerization of actin (Schafer and Schroer, 1999). Consistent with this possibility, BAF53 and β-actin of the mammalian SWI/SNF complex were shown to mediate the formation of branching networks of actin filaments in vitro (Rando *et al.*, 2002). This property would enable BAF53 to play a pivotal role in either the assembly of protein scaffolds between neighboring chromatin fibers or in linking protein scaffolds to chromatin. Considering these properties of BAF53, we speculated that BAF53 could contribute to the polymeric properties and internal meshwork interactions of chromatin fibers through the BAF53-associated chromatin-modifying complexes or the assembly of an actin network.

To begin investigating this possibility, we knocked down BAF53 by small interfering RNA (siRNA) interference and investigated the effects of this action on CTs and chromatin compaction. Our results show that the depletion of BAF53 leads to the expansion of chromosome territories and the decompaction of the chromatin structure. Further, we show that BAF53 knockdown affects the expression of a subset of genes and the progress of cell cycle.

MATERIALS AND METHODS

Synchronization and RNA Interference

To synchronize the NIH3T3 cells in G1/S phase, 5 mM thymidine was added to the medium, and the cells were incubated for 12 h. The cells were washed in phosphate-buffered saline (PBS), and fresh medium was added. After 9 h, 5 mM thymidine was again added to the medium, and the cells were incubated for 14 h. The cells were transfected with siRNA duplexes using siPORTamine (Ambion, Austin TX). The target sequences for the siRNA are listed in the supplementary material (Supplementary Table S1). Trichostatin A treatment was carried out at 50 ng/ml for 5 h.

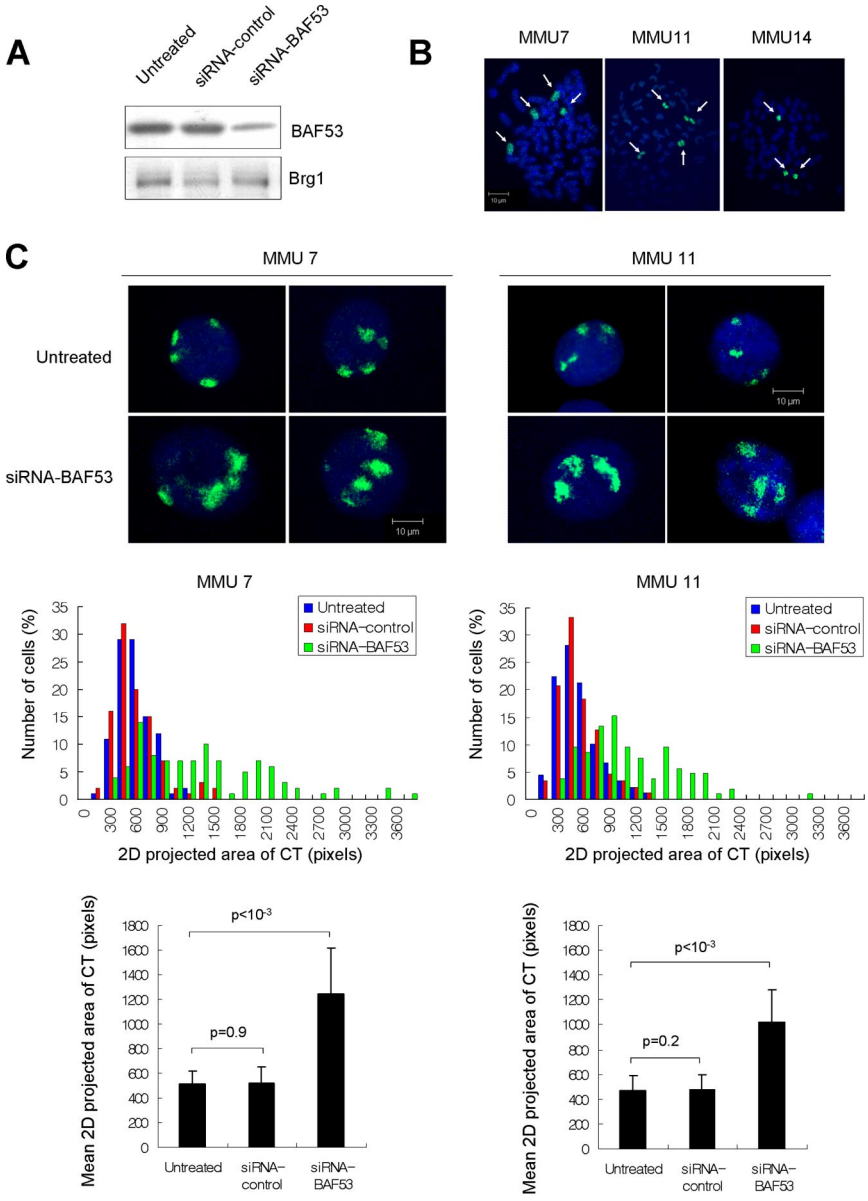

Figure 1. Expansion of chromosome territories by BAF53 knockdown. (A) BAF53 depletion by siRNA interference. NIH3T3 cells were transfected with either siRNA-control or siRNA-BAF53. The extracts were prepared at 48 h after transfection and immunoblotted with BAF53 antibody. Brg1 was used as a loading control. (B) Number of chromosome 7, 11, and 14 in NIH3T3 cells was determined by FISH on metaphase spreads. The chromosome spreads were hybridized with the paints specific for each chromosome. (C) 2D FISH was used to detect MMU7 and MMU11 territories (green). DNA was counterstained with Hoechst 33258 (blue). Bar, 10 μm. Histograms showing the distribution of the projected area and the mean 2D projected area (mean ± SE; n = 100 cells) of MMU7 and MMU11 CTs.

Antibodies

The BAF53 antibody was raised in rabbits using the GST-BAF53(1–155) protein. The BRG-1 antibody and the histone H1 antibody were described in (Clarke *et al.*, 1992; Lee *et al.*, 2002). The antibodies specific for histone modifications were purchased from Upstate Biotechnology (Lake Placed, NY). The mBrm, p21, p27, and Erk2 antibodies were purchased from Santa Cruz Biotechnology (Santa Cruz, CA), and the β-tubulin antibody was purchased from Sigma (St. Louis, MO).

Fluorescence In Situ Hybridization and Image Analysis

Paints for mouse chromosome 7 (MMU7), 11 (MMU11), and 14 (MMU14) were purchased from Cambio Ltd. (Cambridge, United Kingdom). NIH3T3 cells were arrested at the G1/S border by double-thymidine treatment. Two-dimensional (2D) and three-dimensional (3D) fluorescence in situ hybridization (FISH) were carried out as previously described with minor modifications (Mahy *et al.*, 2002; Solovei *et al.*, 2002).

For 2D FISH, the cells were swollen in 0.5% trisodium citrate/0.25% KCl at 37°C for 20 min and then fixed five times with methanol acetic acid (MAA; 3:1, vol/vol). The nuclei were denatured in 70% formamide/2× SSC at 65°C for 2 min, followed by dehydration procedures. The probes were denatured at 65°C for 10 min and were held at 37°C for 1 h before hybridization. The slides were hybridized to paints in 50 mM sodium phosphate/20% dextran sulfate/4× SSC at 37°C overnight. Unbound probes were removed by washing twice each at 45°C for 5 min sequentially with 50% formamide/1× SSC, 2× SSC, and 4× SSC/0.05% Tween-20. Biotinylated probes were detected using avidin-fluorescein isothiocyanate (FITC; Vector Laboratories, Burlingame, CA), followed by biotinylated antiavidin (Vector Laboratories), and finally by avidin-FITC. The slides were then counterstained with Hoechst 33258.

For 3D analysis, cells were fixed in 4% paraformaldehyde in 1× PBS for 10 min at room temperature. After being washed three times with PBS, the cells were permeabilized with a mixture of 0.5% saponin and 0.5% Triton X-100 in PBS for 20 min at room temperature. The cells were incubated in 20% glycerol-PBS for 20 min, and subsequently subjected to five repeated freeze-thaw cycles in liquid N_2. The cells were then treated with 0.1 N HCl for 5 min at room temperature, washed three times with PBS, and stored in 50% formamide in 2× SSC for at least 3 d before hybridization. Cells were denatured in 70% formamide in 2× SSC, pH 7.0, at 73°C for 3 min, followed by 1 min denaturation in 50% formamide in 2× SSC, pH 7.0, at 73°C. Probe hybridization was performed as in the 2D FISH analysis.

The area of the CT in 2D FISH was determined using IPLab for Windows (ver. 3.5.1, Microsoft, Redmond, WA) essentially as previously described

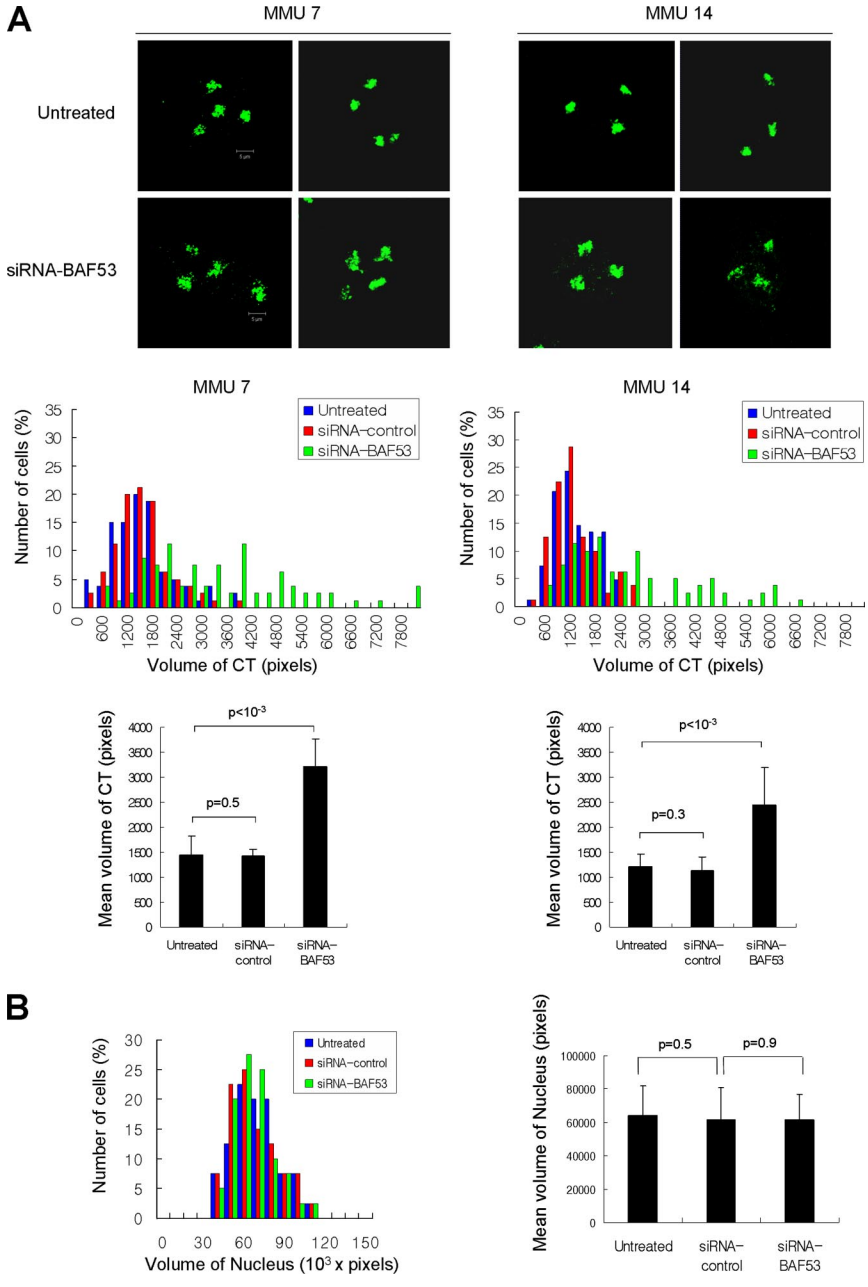

Figure 2. Expansion of chromosome territories by BAF53 knockdown demonstrated by 3D FISH. (A) 3D FISH was used to detect MMU7 and MMU14 territories. Histograms showing the distribution of the volume and the mean volume (mean ± SE; n = 100 cells) of MMU7 and MMU14 CTs. (B) Effect of BAF53 depletion on nuclear volume. The nucleus was visualized by staining with PI, and the volume of nucleus was measured under confocal microscopy. Histogram showing the distribution of the volume of the nuclei. The mean volumes of the nuclei showed no significant difference (mean ± SE; n = 50 cells).

(Mahy *et al.*, 2002). Normalization was performed to remove any background from the FITC images. The hybridization signal was segmented on the basis of pixel thresholding, and a region of interest was manually defined to include all of the detectable territory. The area of the territory was calculated as the number of pixels in a region of interest.

For the quantitative analysis of the volume of the CT in 3D FISH, a series of confocal plane images with a 1-μm z-step were collected using an LSM 510 (Carl Zeiss, Thornwood, NY). The area of CT in each plane was determined in a manner similar to that determined in 2D FISH. The areas of the CTs of all the planes comprising the nucleus, typically 8–12 planes, were summed to give the volume of the CT.

Metaphase spreads of NIH3T3 cells were prepared as previously described (Ono *et al.*, 2003). The statistical analysis of the data were performed using one-way ANOVA, and $p < 0.001$ was considered to be significant.

Micrococcal Nuclease Assay

Cells were permeabilized with LPC buffer (0.01% L-α -lysophosphatidylcholine (Sigma), 150 mM sucrose, 80 mM KCl, 35 mM HEPES, pH 7.4, 5 mM K_2HPO_4, 5 mM $MgCl_2$, and 0.5 mM $CaCl_2$) at room temperature for 90 s. The cells were then digested with 2 U/ml micrococcal nuclease (Sigma) in 20 mM sucrose, 50 mM Tris-HCl, pH 7.5, 50 mM NaCl, and 2 mM $CaCl_2$ at room temperature for various times. Genomic DNA was isolated and subjected to 0.8% agarose electrophoresis. To analyze the nucleosome repeat lengths, 4×10^5 prepermeabilized cells were digested with 2 U/ml (untreated cells) or 0.5 U/ml (BAF53 knockdown cells) for 3 min. Genomic DNA was subjected to 1.5% agarose electrophoresis. SigmaPlot 2004 (Systat Software, Point Richmond, CA) was used to analyze and graph the data.

Fractionation of Chromatin

To isolate the chromatin-nuclear matrix fraction, cells were resuspended in buffer A (10 mM HEPES, pH 7.9, 10 mM KCl, 1.5 mM $MgCl_2$, 0.34 M sucrose, 10% glycerol, 1 mM dithiothreitol [DTT], 5 μg/ml aprotinin, 5 μg/ml leupeptin, 0.5 μg/ml pepstatin, and 0.1 mM phenylmethylsulfonyl fluoride [PMSF]). Triton X-100 was added up to a concentration of 0.1%, and the cells were then incubated for 5 min on ice. The nuclei were collected by centrifugation at 1300 $\times$ *g* for 4 min and washed once with buffer A. To release chromatin-bound proteins by nuclease treatment, the nuclei in buffer A plus 1 mM $CaCl_2$ were digested with 2 U/ml micrococcal nuclease (MNase; Sigma) at 37°C for 10 min. The reaction was terminated upon the addition of 2 mM EGTA. The nuclei were collected by centrifugation at 1300 $\times$ *g* for 4 min and lysed in buffer B (250 mM NaCl, 10 mM HEPES, pH 7.9, 0.34 M sucrose, 3 mM EDTA, 0.2 mM EGTA, and 1 mM DTT) for 30 min on ice. Insoluble chromatin was collected by centrifugation at 1700 $\times$ *g* for 8 min at 4°C, and it was washed once with buffer B.

Electron Microscopy

Samples for negative staining with uranyl acetate were prepared and examined as described (Fan *et al.*, 2005). Cells in 0.5% NP-40 in RSB (10 mM NaCl, 3 mM $MgCl_2$, 1 mM PMSF, and 10 mM Tris-HCl, pH 7.5) were homogenized by 15 strokes (pestle A) over a 20-min period at 4°C. The nuclei were resuspended in RSB containing 1 mM $CaCl_2$, digested with 0.1 U (for the BAF53 knockdown cells) or 0.5 U (for the control cells) of MNase per 2.5×10^6 nuclei for 5 min at 15°C, and terminated by adding 5 mM EGTA. The nuclei were pelleted by centrifugation for 6 min at 1000 $\times$ *g*, resuspended in TEN buffer (10 mM Tris-HCl, pH 7.5, 1 mM EDTA, and 5 mM NaCl), and incubated for 30 min on ice. To remove cell debris, the lysate was centrifuged for 5 min at 4000 $\times$ *g*, and the supernatant was loaded onto 12-ml linear sucrose gradients (5–40% wt/vol) containing TEN buffer and centrifuged in a Beckman SW41 rotor (Fullerton, CA) at 4°C for 12 h at 35,000 rpm. Fractions with chromatin fibers longer than ~20 nucleosomes were combined, dialyzed extensively against HEN buffer (10 mM HEPES, pH 7.4, 1 mM EDTA, and 5 mM NaCl), and concentrated in Centricon filter devices (Millipore, Bedford, MA) 100,000 MW cutoff). Polynucleosomes were fixed by dialysis in 0.1% glutaraldehyde in HEN buffer for 4 h, and glutaraldehyde was then removed by dialysis in HEN buffer alone at 4°C overnight. For negative staining, fixed samples were loaded on glow-discharged formvar-coated copper grids for 20 s. The samples were stained with 2% (wt/vol) aqueous uranyl acetate for 20 s and washed with distilled water. After drying in air for 5 min, the preparations were examined with an energy-filtering transmission electron microscope (LIBRA 120; Carl Zeiss) operated at an accelerating voltage of 120 kV. Zero-loss energy-filtered images were recorded with a 4K slow-scan charge-coupled device camera (4000 SP; Gatan, Pleasanton, CA).

cDNA Microarray

Total RNAs were extracted from the untreated cells and the siRNA-BAF53-transfected cells using the RNeasy kit (Qiagen, Chatsworth, CA). Experiments were independently performed four times with dye swapping. Synthesis of fluorescent-labeled cDNA and the subsequent hybridization to GenePlorer TwinChip Mouse-7.4K arrays were performed by Digital Genomics (http://www.digital-genomics.co.kr/05_info/Microarray02.pdf). Data were analyzed using GenePix software (Axon Instruments, Union City, CA). Significance analysis of microarray (SAM) was performed for the selection of the genes with significant gene expression changes (Tusher *et al.*, 2001).

Proliferation Assay and Flow Cytometry

For the proliferation assay, 5×10^4 cells were plated into a 35-mm dish in triplicate and counted at indicated times. For fluorescence-activated cell sorting (FACS), cells were harvested by trypsinization, washed three times with PBS, and incubated with DNase-free RNase (10 μg/ml) at 37°C for 1 h. Cells were collected by centrifugation at 2000 rpm for 5 min by microcentrifuge and stained with propidium iodide (PI) solution (50 μg/ml PI, 0.1% sodium citrate, 0.3% NP-40, and 50 μg/ml RNase in PBS) at 37°C for 15 min. FACS analyses were performed on the Becton Dickinson Biosciences FACSCalibur (Program: CellQuest, Lincoln Park, NJ). For asynchronous cell population, FACS was performed at 48 h after transfection. For mitosis-blocked cell population, cells were exposed to nocodazole (50 ng/ml) for an additional 24 h before FACS analysis. For biparametric PI and bromodeoxyuridine (BrdU) analysis, cells were labeled with BrdU (20 μM) for 1 h after the release from G1/S arrest. The cells were washed in PBS and a medium without BrdU was added. After 24 h, cells were stained with PI and subjected to FACS analysis.

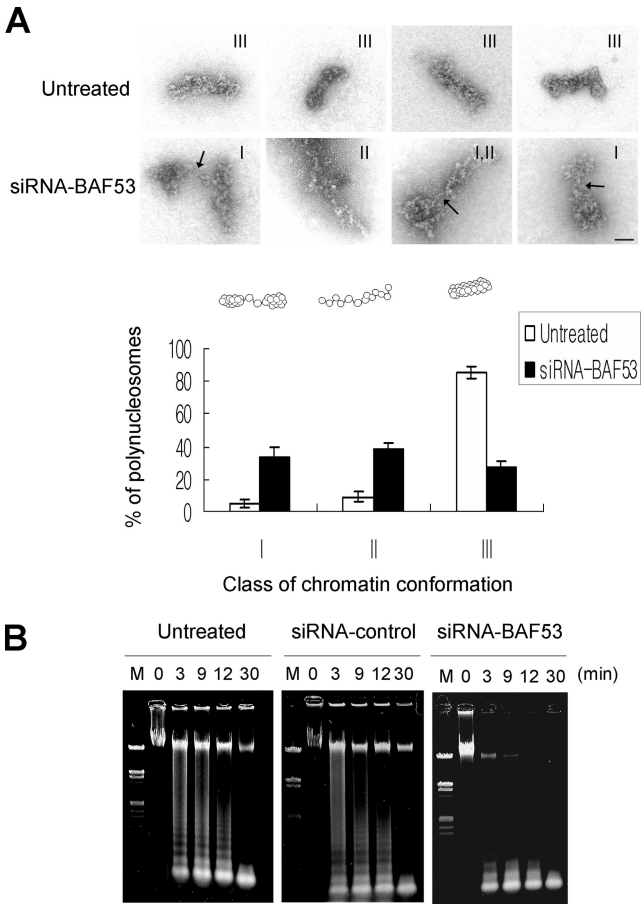

Figure 3. Decompaction of chromatin fiber by BAF53 knockdown. (A) Images of polynucleosomes (n = 20–40) isolated from untreated and BAF53 knockdown cells negatively stained with uranyl acetate. Bar, 50 nm. The "kink" conformation with visible linker DNA (arrow) and heterogeneity are especially striking in the polynucleosomes from the BAF53 knockdown cells. Classification of polynucleosomes in the micrographs according to the "kink" conformation (I), the partial-open conformation with local "beads-on-a-string" (II), and the ordered pattern (III; mean ± SE; n = 40 polynucleosomes). (B) Micrococcal nuclease sensitivity of the chromatin from untreated, siRNA control-transfected, and siRNA-BAF53–transfected cells. Cells, 4×10^5, were detergent-permeabilized 2 d after the transfection and digested with MNase (2 U/ml) for the indicated amount of time. M, lambda DNAs digested with EcoRI and HindIII.

RESULTS

Expansion of Chromosome Territories by BAF53 Depletion

To determine the functional significance of BAF53 for CTs, we examined whether BAF53 depletion led to the expansion of the chromosome territory. We used siRNA interference to suppress BAF53 expression. The level of BAF53 in NIH3T3 cells was reduced to 31% of control levels within 48 h after the addition of specific siRNAs (Figure 1A). Unrelated control siRNAs had no effect on the levels of BAF53. We used 2D and 3D FISH to measure the projected interphase area and volume of CTs from mouse chromosomes 7, 11, and 14 (MMU7, MMU11, MMU14) using the paints specific for each chromosome. NIH3T3 cells are aneuploid and have four MMU7s, four MMU11s, and three MMU14s (Figure 1B). FISH analyses were applied to NIH3T3 cells arrested at the G1/S border by double-thymidine treatment. FACS analyses showed >90% enrichments of G1 phase cells in these preparations (see Supplementary Figure S1). Four MMU7-, four MMU11-, and three MMU14-CTs could be clearly discerned in both the 2D and 3D FISH analyses.

When BAF53 was knocked down by BAF53-specific siRNA, the 2D projected areas of the CTs for MMU7 and MMU11 showed a dramatic change: the mean 2D projected area increased by 2.4- and 2.2-fold in MMU7 and MMU11, respectively (Figure 1C). The CTs of the siRNA control-transfected cells were indistinguishable from the CTs of the untreated cells. We obtained a similar increase in the 2D projected area of MMU7 using another BAF53-specific siRNA, siRNA-BAF53(II) (see Supplementary Figure S2).

The increase in the 2D projected area could be due to flattening of the nuclei. To exclude this possibility, we examined the changes in the CT volume in 3D-preserved preparations. Consistent with results of the 2D FISH analysis, the mean volume of the CTs in the BAF53 knockdown cells increased by 2.2- and 2.0-fold in MMU7 and MMU14, respectively (Figure 2A). The volumes of the nuclei measured by PI staining were not significantly changed by BAF53 knockdown (Figure 2B). Taken together, these results clearly demonstrate that BAF53 knockdown leads to the expansion of chromosome territories.

BAF53 Depletion Causes Reductions in Chromatin Compaction

To investigate whether the observed changes in the CTs could have originated from alterations in chromatin compaction, we isolated polynucleosomes (n = 20–40) from untreated control cells and BAF53 knockdown cells and examined them under electron microscopy (Figure 3A). The chromatin isolated from the untreated cells exhibited a regular, helical organization, which was characteristic of the 30-nm fiber. On the other hand, the chromatin isolated from the BAF53 knockdown cells appeared to be less compact and highly irregular. A "kink" conformation with visible linker DNA and a partial-open conformation with local "beads-on-a-string" were commonly found in the chromatin isolated

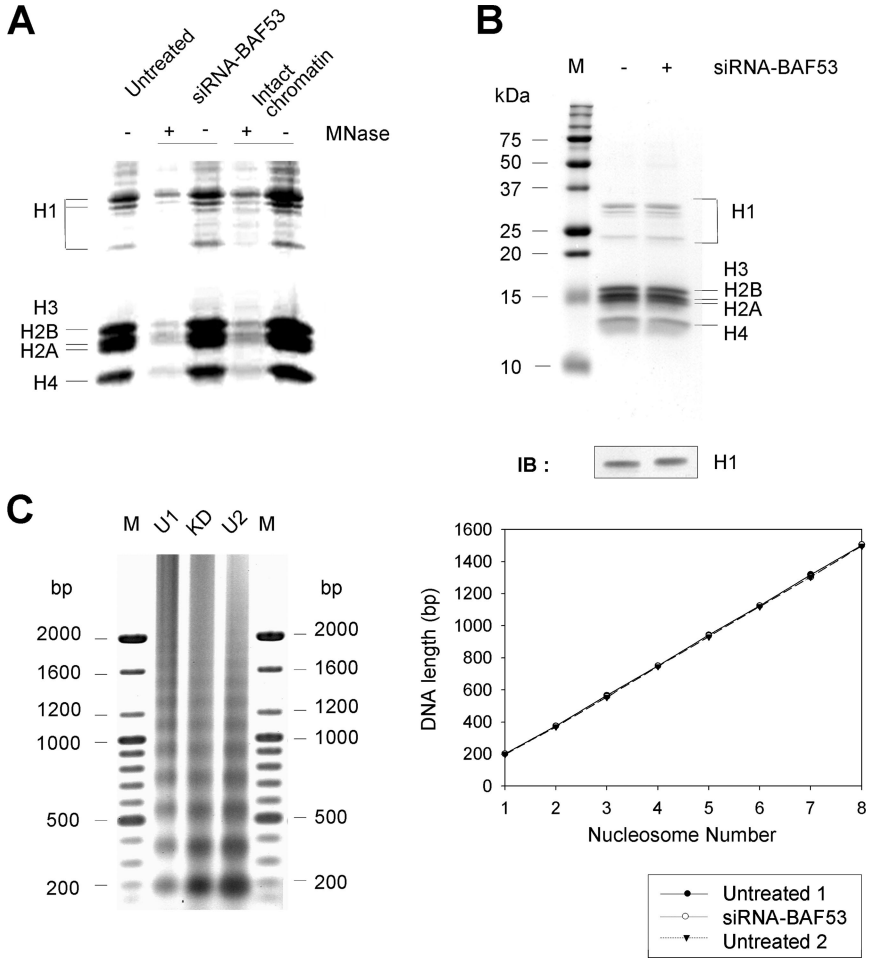

Figure 4. BAF53 depletion affects neither chromatin loading of H1 nor nucleosome repeat length. The levels and composition of H1 and core histones were analyzed by SDS-PAGE and Coomassie brilliant blue staining or immunoblotting (IB) with H1 antibody. (A) At day 2 after transfection, the chromatin-nuclear matrix fraction was isolated with (+) or without (−) MNase treatment. Detergent-permeabilized and low-salt–extracted cells served as the intact chromatin. (B) Polynucleosomes (n = 20–40) were isolated from MNase-digested cells by sucrose gradient centrifugation. (C) Nucleosome repeat length from bulk chromatin. MNase digests of untreated (U1 and U2) and BAF53 knockdown (KD) cells after detergent-permeabilization. M, DNA markers. Compared with KD, the digestion was less extensive for U1 and more extensive for U2. Plot of nucleosome number versus DNA length and linear regression analysis of data points.

from the BAF53 knockdown cells; however, they were rarely seen in the chromatin isolated from the untreated cells.

Chromatin decompaction by BAF53 depletion was supported by an MNase sensitivity analysis. MNase treatment of detergent-permeabilized cells results in the progressive digestion of chromatin, which produces a ladder of numerous DNA bands (Figure 3B). The near-complete conversion of the chromatin from untreated cells into mono- or dinucleosomes took 30 min under the used conditions. On the other hand, the near-complete conversion of the chromatin from the BAF53 knockdown cells into mono- or dinucleosomes was completed within just 3 min. Transfection with siRNA-control did not alter the rate of digestion. Considering that MNase cuts chromatin in the linker region between nucleosomes, this result indicates that the conformational alteration of chromatin by BAF53 depletion is dramatic enough to expose the linker regions to MNase.

No Alteration in Histone Composition and Nucleosome Repeat Length in BAF53 Knockdown Cells

Linker histone H1 plays a central role in the folding of chromatin into a 30-nm fiber. We isolated chromatin-enriched fractions from untreated cells and BAF53 knockdown cells, and we compared the relative levels of H1 and core histones between the two cell types in order to investigate whether a reduction in the chromatin loading of H1 could be responsible for the chromatin decompaction by BAF53 depletion. We could not detect any discernible reduction in H1 and core histone levels in the chromatin-nuclear matrix fraction of BAF53 knockdown cells (Figure 4A). We also did not observe any difference in the molar ratio of the H1 molecule to core histones between the polynucleosomes isolated from the untreated and BAF53 knockdown cells (Figure 4B).

H1 depletion has been shown to reduce nucleosome repeat length by 15 base pairs (Fan *et al.*, 2005). We digested detergent-permeabilized control and BAF53 knockdown cells with MNase and measured the nucleosome repeat length of each cell. The control and BAF53 knockdown cells had similar nucleosome repeat lengths of 187 and 186 base pairs, respectively, showing clean linear relationships between nucleosome number and DNA length (Figure 4C). The nucleosome repeat length of the control cells did not change with more extensive digestion. Taken together, these results demonstrate that BAF53 depletion does not eliminate H1 and core histones from chromatin.

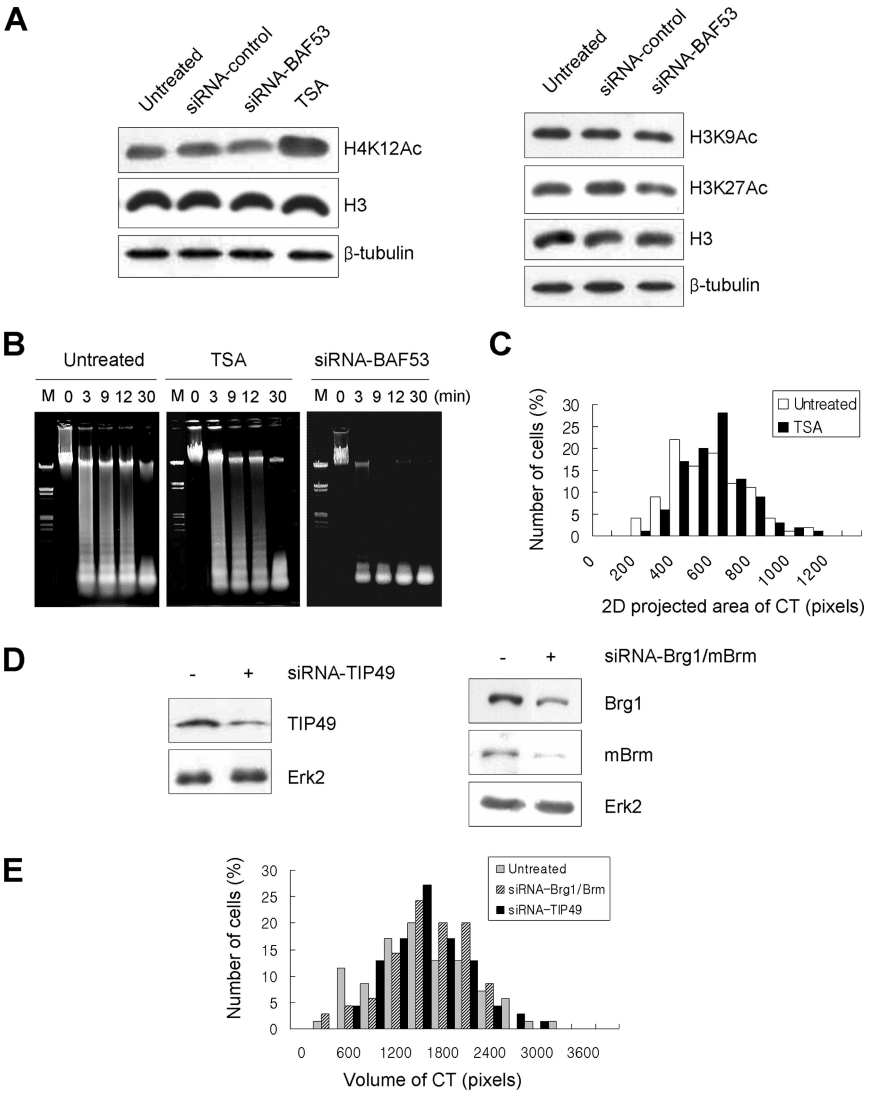

Figure 5. Effects of chromatin hyperacetylation and knockdown of BRG-1, mBrm, and Tip49 on CTs. (A) Immunoblotting analysis on lysates from untreated, siRNA control-transfected, siRNA-BAF53–transfected, and TSA-treated cells. β-tubulin was used as a loading control. (B) Micrococcal nuclease sensitivity of the chromatin was determined as described in Figure 3. M, lambda DNAs digested with EcoRI and HindIII. (C) The distribution of MMU7 CT area for untreated and TSA-treated cells detected by 2D FISH. (D) BRG-1, mBrm, and Tip49 level after siRNA interference was analyzed by immunoblotting analysis. BRG-1 and mBrm were concurrently knocked down by cotransfection with siRNA-BRG-1 and siRNA-mBrm. (E) The distribution of MMU7 CT volume for untreated, BRG1/mBrm knockdown, and Tip49 knockdown cells detected by 3D FISH.

Neither Hyperacetylation nor Down-Regulation of BRG-1 and mBrm Leads to the Expansion of CTs

Because histone acetylation leads to the "open" chromatin structure and the BAF53-containing TIP60 complex exhibits HAT activity (Ikura *et al.*, 2000), we examined whether histone acetylation could be responsible for the chromatin transition observed in the BAF53 knockdown cells. No significant changes in the levels of H4-K12, H3-K9, and H3-K27 acetylation were detected in the BAF53 knockdown cells (Figure 5A). When the hyperacetylation of histones was induced by treatment with trichostatin A, the MNase sensitivity and the area of the MMU7 CTs were not altered as dramatically as in the case of BAF53 knockdown (Figure 5, B and C).

We then explored the possibility that the effect of BAF53 depletion on the chromatin transition was mediated by the suppression of the SWI/SNF complex. We down-regulated both BRG-1 and mBrm, the catalytic core subunits of the SWI/SNF complex, by siRNA interference and examined their effect on MMU7 CTs using 3D FISH. The down-regulation of BRG-1 and mBrm did not increase the volume of MMU7 CTs (Figure 5, D and E). We also found that the down-regulation of Tip49, a potential helicase component of the TIP60 complex, did not alter the MMU7 CTs (Figure 5, D and E).

BAF53 Knockdown Causes Alterations in H3-K9 and H3-K79 Dimethylation

We next examined whether BAF53 knockdown is accompanied with changes in distinct histone lysine methylation. Immunoblotting analysis showed that H3-K9 dimethylation decreased and H3-K79 dimethylation increased in the BAF53 knockdown cells, whereas other histone lysine methylations including H3-K9 mono- and trimethylation remained unchanged (Figure 6A). Supporting results were obtained in immunofluorescence experiments (Figure 6B). The staining intensity of H3-K9 dimethylation was significantly reduced in the BAF53 knockdown cells. On the other hand, the overall signal for H3-K9 monomethylation and trimethylation remained unchanged by BAF53 depletion. It is noteworthy that H3-K9 dimethylation foci remained clearly visible at the nuclear periphery and the pericentric heterochromatin periphery in spite of a general reduction of H3-K9 dimethylation.

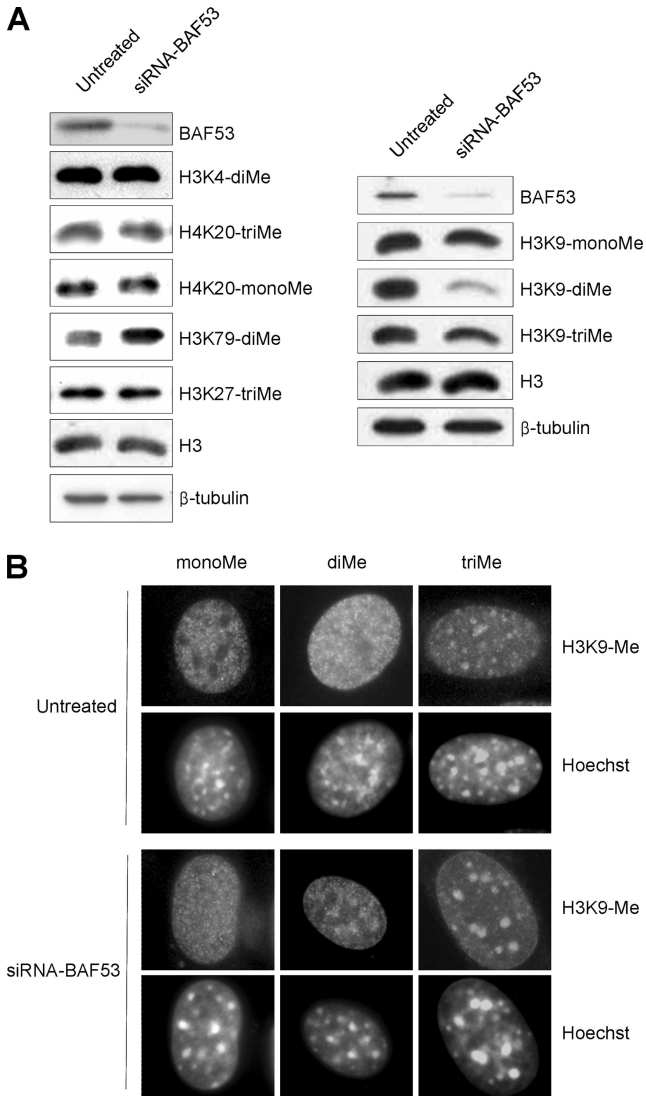

Figure 6. BAF53 knockdown leads to a reduction of H3-K9 dimethylation, whereas an increase of H3-K79 methylation. (A) Immunoblotting analysis using antibodies specific for the indicated histone modifications on lysates from untreated and siRNA BAF53–transfected cells. Blottings with BAF53 and β-tubulin antibody were performed to confirm BAF53 knockdown and equal loading. (B) Immunofluorescence staining in untreated and siRNA BAF53–transfected cells with antibodies specific for the indicated histone modifications.

BAF53 Knockdown Leads to Up-Regulation of Cell Cycle Regulator Genes and a Defect in Cell Cycle Progression

It is of great interest to determine how gene expression is affected in the genomic level by the decompaction of the chromatin structure in the BAF53 knockdown cells. Therefore, we compared the gene-expression profile of the untreated and BAF53 knockdown cells by a cDNA array study. Genes were determined to show significant changes in expression when they satisfied both of the following conditions: 1) the difference in gene expression was greater than 1.6-fold and 2) the false discovery rate was $<0.5\%$ in SAM with the data from four independent experiments (Tusher *et al.*, 2001). Among 7400 targets examined, 47 genes could be classified as up-regulated by the BAF53 depletion, but eight genes could be classified as down-regulated (Table 1). This shows that there were more up-regulated genes than down-regulated genes. It is noteworthy that *Xist* and *Hprt1*, two X-linked genes, and *Prm2*, a haploid, male-specific gene are included in the up-regulated genes. We confirmed the up-regulation of the *Prm2*, *Xist*, and *Mdm2* genes by real time RT-PCR (see Supplementary Figure S3).

Interestingly, the transcripts of several cell cycle regulators, such as *Mdm2*, *Cdkn1a* (p21), *Ccnd1* (cyclin D1), and *Dusp1*, were highly induced in the BAF53 knockdown cells. It raises a possibility that the alteration in the higher-order chromatin structure by BAF53 knockdown leads to a stress or cell cycle check point response. To address this issue, we monitored the proliferative properties of the BAF53 knockdown cells by growth curves analysis. Although the control population grew steadily after transfection, the number of BAF53 knockdown cells ceased to increase from 24 h after transfection (Figures 7A). We next monitored the DNA content of the transfected cells by FACS analysis after staining of the DNA with PI (Figure 7C). The cell cycle profile of the BAF53 knockdown cells progressively right-shifted and broadened. We next tested whether the BAF53 knockdown cells are able to complete cell cycle. We treated asynchronous cells with nocodazole for 24 h before FACS analysis. As expected, the control cells accumulated in G2(4N DNA con-

Table 1. Genes up- and down-regulated by BAF53 knockdown

Genes up-regulated				
			Relative expression	
Accession number	Gene name	Description	Microarray (*-fold*)	Real-time RT-PCR
Transcription				
NM_009236	Sox18	SRY-box containing gene 18	2.89	
NM_008933	Prm2	Protamine 2	2.80[a]	3.5 ± 0.3
L04961	Xist	Inactive X-specific transcripts	1.66[a]	4.6 ± 0.4
Cell cycle				
NM_010786	Mdm2	Transformed mouse 3T3 cell double minute 2	3.62[a]	12.3 ± 0.4
NM_013642	Dusp1	Dual specificity phosphatase 1	2.95	
NM_007669.2	Cdkn1a	Cyclin-dependent kinase inhibitor 1A (P21)	2.74[b]	
NM_152804	Plk2	Polo-like kinase 2 (Drosophila)	1.98	
NM_007631	Ccnd1	Cyclin D1	1.62	
Signal transduction				
NM_080428	Fbxw7	F-box and WD-40 domain protein 7, archipelago homolog	3.18	
NM_016719	Grb14	Growth factor receptor bound protein 14	1.83	
NM_022019	Dusp10	Dual specificity phosphatase 10	1.77	
NM_016721	Iqgap1	IQ motif containing GTPase-activating protein 1	1.77	
NM_010637	Klf4	Kruppel-like factor 4 (gut)	1.61	
Immune response				
NM_013556.1	Hprt1	Hypoxanthine guanine phosphoribosyl transferase 1	1.72	
Apoptosis				
O55003	Bnip3	BCL2/adenovirus E1B 19 kDa-interacting protein 1, NIP3	4.34	
Response to stress				
NM_010171.2	F3	Coagulation factor III	2.05	
Cellular physiological process				
NM_010357.1	Gsta4	Glutathione *S*-transferase, alpha 4	4.35	
XM_620148.1	Egfl3	EGF-like-domain, multiple 3	3.00	
NM_007899.1	Ecm1	Extracellular matrix protein 1	2.18	
NM_008969.1	Ptgs1	Prostaglandin-endoperoxide synthase 1	2.16	
NM_144792.3	Tmem23	Transmembrane protein 23	2.11	
NM_008127.3	Gjb4	Gap junction membrane channel protein beta 4	2.08	
NM_001001978.1	LOC380687	Similar to glyceraldehyde-3-phosphate dehydrogenase	2.06	
NM_009393.1	Tnnc1	Troponin C, cardiac/slow skeletal	1.98	
NM_009112.1	S100a10	S100 calcium-binding protein A10 (calpactin)	1.96	
NM_007688.1	Cfl2	Cofilin 2, muscle	1.93	
NM_013569.1	Kcnh2	Potassium voltage-gated channel, subfamily H (eag-related), member 2	1.91	
NM_011018.1	Sqstm1	Sequestosome 1	1.90	
NM_010128.3	Emp1	Epithelial membrane protein 1	1.84	
NM_016903	Esd	Esterase D/formylglutathione hydrolase	1.82	
NM_013709.2	Sh3yl1	Sh3 domain YSC-like 1	1.79	
NM_001024604.1	Ankrd28	Ankyrin repeat domain 28	1.79	
NM_026993.1	Ddah1	Dimethylarginine dimethylaminohydrolase 1	1.77	
NM_007438.3	Aldoa	Aldolase 1, A isoform	1.76	
NM_021895.2	Actn4	Actinin alpha 4	1.75	
NM_011593.1	Timp1	Tissue inhibitor of metalloproteinase 1	1.75	
NM_133654.1	Cd34	CD34 antigen	1.74	
NM_011311.1	S100a4	S100 calcium-binding protein A4	1.72	
NM_008133.2	Glud1	Glutamate dehydrogenase 1	1.70	
NM_009842.1	Cd151	CD151 antigen	1.69	
NM_008113.2	Arhgdig	Rho GDP dissociation inhibitor (GDI) gamma	1.67	
NM_008536.2	Tm4sf1	Transmembrane 4 superfamily member 1	1.66	
NM_021536.5	Rhot1	Ras homolog gene family, member T1	1.64	
AB195430.1	D7Ertd458e	DNA segment, Chr 7, ERATO Doi 458, expressed	1.63	
NM_010847.2	Mxi1	Max interacting protein 1	1.62	
NM_007653.2	Cd63	Cd63 antigen	1.60	
NM_146120.2	Gsn	Gelsolin	1.60	

Continued

Table 1. *Continued*

Genes down-regulated				
			Relative expression	
Accession number	Gene name	Description	Microarray (*-fold*)	Real-time RT-PCR
Cell cycle				
NM_008086.1	Gas1	Growth arrest–specific 1	2.08	
Signal transduction				
NM_178804.2	Slit2	Slit homolog 2 (*Drosophila*)	1.85	
Cellular physiological process				
NM_053185.1	Col4a6	Procollagen, type IV, alpha 6	2.07	
NM_032000.1	Trps1	Trichorhinophalangeal syndrome I (human)	1.86	
NM_009041.1	Rdx	Radixin	1.81	
NM_011581.1	Thbs2	Thrombospondin 2	1.8	
NM_009263.1	Spp1	Secreted phosphoprotein 1	1.8	
NM_018865.1	Wisp1	WNT1 inducible signaling pathway protein 1	1.72	

NIH3T3 cells were transfected with siRNA-BAF53 or were left untreated. Total RNAs were extracted, labeled, and hybridized to GenePlorer TwinChip Mouse-7.4K arrays as described in *Materials and Methods.* The fold change in gene expression was determined by comparison of mean average difference scores. Only genes with a fold change in gene expression higher than 1.6-fold and a q value <0.5% in significance analysis of microarray (SAM) with the four independent experimental data are shown.

[a] Genes confirmed by real-time RT-PCR. (See Supplementary Figure S3.)

[b] Gene confirmed by immunoblotting (Figure 7E).

tent), reaching greater than 84%. Less than 12% of control cells remained in G1(2N DNA content), and few S phase cells were found. In contrast, G2 cells largely decreased to 40% in the BAF53 knockdown population. Fifty-three percent of cells were found with the DNA content between 2N and 4N. We next followed the cell cycle progression of newly replicated cells. Replicating cells were labeled with BrdU for 1 h after the release from G1/S arrest and were subjected to FACS analysis after 24 h. Biparametric PI and BrdU analysis shows that most of control cells labeled with BrdU entered to another round of S phase (Figure 7D). On the other hand, a significant portion of BAF53 knockdown cells labeled with BrdU were arrested at G1 but not at G2/M. Taken together, we concluded that the BAF53 knockdown cells were arrested at G1/S border. The induction of p21 and p27 supports that the BAF53 knockdown cells experienced the G1/S checkpoint (Figure 7E).

DISCUSSION

The most striking effect of BAF53 depletion on chromatin structure was a twofold expansion of the CTs, accompanied by widespread decompaction of the chromatin structure. The decompaction of the chromatin structure certainly increases the contour length of the chromatin. Although the increase in contour length would result in an increase in the envelope volume, assuming that the chromatin behaves as an ideal fiber, we are uncertain whether the decompaction of the chromatin structure by BAF53 depletion can solely account for the expansion of CTs. The decompaction of the chromatin structure inevitably alters the stiffness and interactions of the internal meshwork of the chromatin, which cannot be estimated or predicted at the present time. Therefore, the possible negative effect on CTs by alterations in stiffness and in the interactions of the internal meshwork could offset or even override the positive effect of the increase in contour length.

Given that the interactions of the internal meshwork constitute another important parameter determining envelope volume, we should consider the possibility that BAF53 depletion decreases the "caging" force that results from internal meshwork interactions. The BAF53/β-actin component of the SWI/SNF complex is able to cap the pointed-end of F-actin and form a branched actin network (Rando *et al.*, 2002). When β-actin polymerization was permitted in the presence of the SWI/SNF complex, BAF53 and β-actin mediated the binding of the complex to the pointed-end of the actin filaments, and some of these proteins also attached filaments to the sides of other filaments to create branch points. This dynamic BAF53-regulated actin network may contribute to the internal meshwork interactions between nucleosome-nucleosome or nucleosome-protein scaffolds. This phenomenon is reminiscent of the formation of branching networks of actin filaments by the Arp2/3 complex at the leading edge of migrating cells (Mullins *et al.*, 1998).

Both the multiloop subcompartment model and the chromonema model posit that the interactions of the internal meshwork provide major driving forces for large-scale chromatin folding and eventually the formation of a chromosomal subdomain. Disruptions of the internal meshwork interactions would lead to the disintegration of chromosomal subdomains. The characteristic features of a tertiary chromatin structure derived from artificial tandem arrays and natural chromosomes are "beaded" images observed by light microscopy (Muller *et al.*, 2004). It will be of great interest to investigate whether these beaded domains are preserved when BAF53 is suppressed.

The irregularity and decompaction of the polynucleosomes isolated from the BAF53 knockdown cells are similar to those observed from the H1-depleted cells (Fan *et al.*, 2005). On the other hand, the chromatin loading of H1 and core histones remained unaltered in the BAF53 knockdown cells. Little change in nucleosome repeat length indicates that the H1 histones properly contacted the DNA helix that had exited the nucleosome core particle. This suggests that the structural transitions caused by BAF53 knockdown and H1 depletion are fundamentally distinct and that the stability of the 30-nm fiber depends on other factor(s) in addition

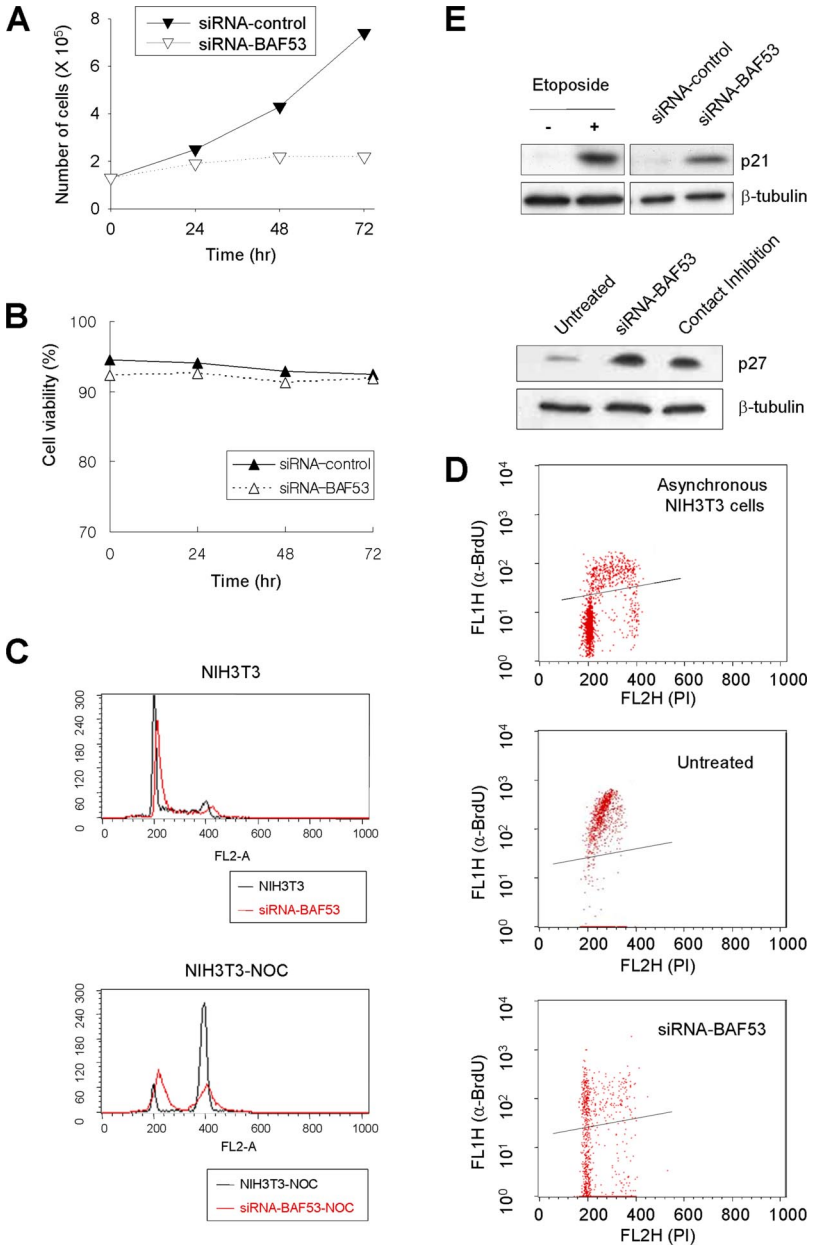

Figure 7. Cell cycle defect by BAF53 knockdown. (A) NIH3T3 cells were transfected with either siRNA-control or siRNA-BAF53, and cell numbers were counted after the indicated amount of time. Cells, 0.5×10^5, were initially plated a day before transfection. (B) Cell viability analysis. NIH3T3 cells were transfected with either siRNA-control or siRNA-BAF53, and cells were stained with 0.4% trypan blue after the indicated amount of time. (C) FACS analysis after staining of the DNA with PI. At 48 h after transfection, FACS was performed for the asynchronous cell population (top) or the mitosis-blocked cell population, which was exposed to nocodazole for an additional 24 h (bottom). (D) Biparametric PI and BrdU analysis. Asynchronous NIH3T3 cells were labeled with BrdU (20 μM) for 20 min before FACS analysis (top). Untreated (middle) and BAF53 knockdown cells (bottom) were labeled with BrdU (20 μM) for 1 h after the release from G1/S arrest. Cells were washed and incubated in a medium without BrdU for 24 h before FACS analysis. FACS analysis was performed after staining of the DNA with PI. (E) Immunoblotting analysis using the p21 and p27 antibody on lysates from siRNA-control transfected and siRNA-BAF53 transfected cells. Etoposide (100 μM for 2 h) was used as a positive control for the induction of p21. p27 was induced by contact inhibition.

to the binding of H1. Histone modification, DNA methylation, and the association of nonhistone architectural components could be considered as potential modulators of the 30-nm fiber structure. In this study we found that BAF53 knockdown led to the decrease of H3-K9 dimethylation and the increase of H3-K79 dimethylation. H3-K9 and H3-K79 methylation are two key histone modifications closely linked to the formation of silent chromatic regions with the opposite behaviors: H3-K9 is hypermethylated and H3-K79 is hypomethylated in silent chromatic regions (Ng *et al.*, 2003; Noma *et al.*, 2001). The hypermethylated H3-K9 and the hypomethylated H3-K79 could promote the association of nonhistone architectural proteins such as HP1 making the chromatin more compact. Therefore, the suppression of this process by the reduction of H3-K9 dimethylation and the increase of H3-K79 dimethylation may contribute to the decompaction of the chromatin in the BAF53 knockdown cells. On the contrary, we cannot exclude the possibility that the alterations in H3-K9 and H3-K79 dimethylation result from the decompaction of the chromatin.

Despite the global changes in chromatin structure present in the BAF53 knockdown cells, very few genes exhibited the difference in gene expression by 1.6-fold or more. It is, however, not surprising because it turns out that the alteration in global chromatin structure does not result in the profound change in the gene-expression profile (Fan *et al.*, 2005). The depletion of linker histone H1 caused the decrease in nucleosome spacing and chromatin compaction throughout the genome. However, only $<0.3\%$ of genes showed expression differences of twofold or more. Although the decompaction of the chromatin structure may open the closed-chromatin conformation, it alone appears to be not sufficient to initiate transcription. The required transcriptional transacting-factors must be provided for transcription to take place.

Intriguingly BAF53 knockdown leads to cell cycle arrest in G1 phase. Induction of the transcripts of several cell cycle regulators such as Mdm2, p21, cyclin D1, and Dusp1 supports this observation. Deregulation of these genes could be due to derepression of silent euchromatic regions. Alternatively it is plausible that the disruption of the higher-order organization of chromatin initiate intracellular stress responses resulting in cell cycle arrest, as chromosomal structural changes resulting from treatment with chloroquine, trichostatin A, or hypotonic conditions activates DNA double strand break response (Bakkenist and Kastan, 2003).

Temperature-sensitive mutants of Arp4 and Alp5, budding and fission yeast homology of BAF53 respectively, suffer from defects in G2/M phase function (Minoda *et al.*, 2005; Ogiwara *et al.*, 2007). It has been suggested that Arp4p and Alp5p function in the assembly of kinetochores via the Arp4p- or Alp5-containing complexes such as INO80, NuA4, SWR1 complex in budding yeast and Mst1 complex in fission yeast. On the contrary, BAF53 knockdown cells do not show a defect in G2/M phase. In mammals, genome evolution may exempt BAF53 from its role in the assembly of kinetochores. On the other hand, we do not exclude the possibility that the incomplete knockdown of BAF53 allows the escape from mitotic phenotypes. It is noteworthy that some of *arp4* mutants display a defect in the transition from G1 to S phase suggesting that *arp4* mutants may experience the similar defects with BAF53 knockdown cells (Ogiwara *et al.*, 2007).

The molecular process by which BAF53 depletion leads to chromatin fiber decompaction remains to be elucidated. Considering that BAF53 is an essential protein required for the assembly of several chromatin remodeling and modifying complexes (Galarneau *et al.*, 2000; Sunada *et al.*, 2005), suppression of BAF53-associated complexes can be conceived as an initial event. Alternatively, the disruption of the higher-order organization of chromatin may be directly linked to this process. It has been proposed that the constraint posed by a closely packed internal meshwork may promote a more compact conformation of chromatin or higher-organization processes, such as the development of chromatin loops (Kleckner *et al.*, 2004). The proposed compact conformation of chromatin or chromatin loops may facilitate the loading of nonhistone architectural components, the exchange with histone variants, or the recruitment of chromatin modifying complexes.

ACKNOWLEDGMENTS

This work is supported by the Basic Research Program of the Korea Science and Engineering Foundation (R01–2002-000-00373-0 to H.K.), the Brain Research Center of the 21C Frontier Research program of the Ministry of Science and Technology (M103KV010007-06K2201-00710 to Y.K.K.), the Korea Health 21R&D Project of the Ministry of Health and Welfare (A04-0018-AY1204-06A3-00020B to Y.K.K.), and the BK21 of the Ministry of Education (to Y.K.K.). K.L. is the recipient of the Seoul Science Fellowship.

REFERENCES

Bakkenist, C. J., and Kastan, M. B. (2003). DNA damage activates ATM through intermolecular autophosphorylation and dimer dissociation. Nature *421*, 499–506.

Belmont, A. S., and Bruce, K. (1994). Visualization of G1 chromosomes: a folded, twisted, supercoiled chromonema model of interphase chromatid structure. J. Cell Biol. *127*, 287–302.

Clarke, H. J., Oblin, C., and Bustin, M. (1992). Developmental regulation of chromatin composition during mouse embryogenesis: somatic histone H1 is first detectable at the 4-cell stage. Development *115*, 791–799.

Cremer, T., and Cremer, C. (2001). Chromosome territories, nuclear architecture and gene regulation in mammalian cells. Nat. Rev. Genet. *2*, 292–301.

Fan, Y., Nikitina, T., Zhao, J., Fleury, T. J., Bhattacharyya, R., Bouhassira, E. E., Stein, A., Woodcock, C. L., and Skoultchi, A. I. (2005). Histone H1 depletion in mammals alters global chromatin structure but causes specific changes in gene regulation. Cell *123*, 1199–1212.

Galarneau, L., Nourani, A., Boudreault, A. A., Zhang, Y., Heliot, L., Allard, S., Savard, J., Lane, W. S., Stillman, D. J., and Cote, J. (2000). Multiple links between the NuA4 histone acetyltransferase complex and epigenetic control of transcription. Mol. Cell *5*, 927–937.

Ikura, T., Ogryzko, V. V., Grigoriev, M., Groisman, R., Wang, J., Horikoshi, M., Scully, R., Qin, J., and Nakatani, Y. (2000). Involvement of the TIP60 histone acetylase complex in DNA repair and apoptosis. Cell *102*, 463–473.

Kleckner, N., Zickler, D., Jones, G. H., Dekker, J., Padmore, R., Henle, J., and Hutchinson, J. (2004). A mechanical basis for chromosome function. Proc. Natl. Acad. Sci. USA *101*, 12592–12597.

Kwon, H., Imbalzano, A. N., Khavari, P. A., Kingston, R. E., and Green, M. R. (1994). Nucleosome disruption and enhancement of activator binding by a human SWI/SNF complex. Nature *370*, 477–481.

Lee, D., Lim, C., Seo, T., Kown, H., Min, H., and Choe, J. (2002). The viral oncogene human papillomavirus E7 deregulates transcriptional silencing by Brm-related gene 1 via molecular interactions. J. Biol. Chem. *277*, 48842–48848.

Mahy, N. L., Perry, P. E., Gilchrist, S., Baldock, R. A., and Bickmore, W. A. (2002). Spatial organization of active and inactive genes and noncoding DNA within chromosome territories. J. Cell Biol. *157*, 579–589.

Minoda, A., Saitoh, S., Takahashi, K., and Toda, T. (2005). BAF53/Arp4 homolog Alp5 in fission yeast is required for histone H4 acetylation, kinetochore-spindle attachment, and gene silencing at centromere. Mol. Biol. Cell *16*, 316–327.

Muller, W. G., Rieder, D., Kreth, G., Cremer, C., Trajanoski, Z., and McNally, J. G. (2004). Pi-by-no features of tertiary chromatin structure as detected in natural chromosomes. Mol. Cell. Biol. *24*, 9359–9370.

Mullins, R. D., Heuser, J. A., and Pollard, T. D. (1998). The interaction of Arp2/3 complex with actin: Nucleation, high affinity pointed end capping, and formation of branching networks of filaments. Proc. Natl. Acad. Sci. USA *95*, 6181–6186.

Munkel, C., Eils, R., Dietzel, S., Zink, D., Mehring, C., Wedemann, G., Cremer, T., and Langowski, J. (1999). Compartmentalization of interphase chromosomes observed in simulation and experiment. J. Mol. Biol. *285*, 1053–1065.

Ng, H. H., Ciccone, D. N., Morshead, K. B., Oettinger, M. A., and Struhl, K. (2003). Lysine-79 of histone H3 is hypomethylated at silenced loci in yeast and mammalian cells: a potential mechanism for position-effect variegation. Proc. Natl. Acad. Sci. USA *100*, 1820–1825.

Noma, K., Allis, C. D., and Grewal, S. I. (2001). Transitions in distinct histone H3 methylation patterns at the heterochromatin domain boundaries. Science *293*, 1150–1155.

Ogiwara, H., Ui, A., Kawashima, S., Kugou, K., Onoda, F., Iwahashi, H., Harata, M., Ohta, K., Enomoto, T., and Seki, M. (2007). Actin-related protein Arp4 functions in kinetochore assembly. Nucleic Acids Res. *35*, 3109–3117.

Ono, T., Losada, A., Hirano, M., Myers, M. P., Neuwald, A. F., and Hirano, T. (2003). Differential contributions of condensin I and condensin II to mitotic chromosome architecture in vertebrate cells. Cell *115*, 109–121.

Rando, O. J., Zhao, K., Janmey, P., and Crabtree, G. R. (2002). Phosphatidylinositol-dependent actin filament binding by the SWI/SNF-like BAF chromatin remodeling complex. Proc. Natl. Acad. Sci. USA *99*, 2824–2829.

Schafer, D. A., and Schroer, T. A. (1999). Actin-related proteins. Annu. Rev. Cell Dev. Biol. *15*, 341–363.

Schardin, M., Cremer, T., Hager, H. D., and Lang, M. (1985). Specific staining of human chromosomes in Chinese hamster x man hybrid cell lines demonstrates interphase chromosome territories. Hum. Genet. *71*, 281–287.

Solovei, I., Cavallo, A., Schermelleh, L., Jaunin, F., Scasselati, C., Cmarko, D., Cremer, C., Fakan, S., and Cremer, T. (2002). Spatial preservation of nuclear chromatin architecture during three-dimensional fluorescence in situ hybridization (3D-FISH). Exp. Cell Res. *276*, 10–23.

Sunada, R., Gorzer, I., Oma, Y., Yoshida, T., Suka, N., Wintersberger, U., and Harata, M. (2005). The nuclear actin-related protein Act3p/Arp4p is involved in the dynamics of chromatin-modulating complexes. Yeast *22*, 753–768.

Tusher, V. G., Tibshirani, R., and Chu, G. (2001). Significance analysis of microarrays applied to the ionizing radiation response. Proc. Natl. Acad. Sci. USA *98*, 5116–5121.

Zhao, K., Wang, W., Rando, O. J., Xue, Y., Swiderek, K., Kuo, A., and Crabtree, G. R. (1998). Rapid and phosphoinositol-dependent binding of the SWI/SNF-like BAF complex to chromatin after T lymphocyte receptor signaling. Cell *95*, 625–636.